UNIVERSITÀ POLITECNICA DELLE MARCHE
Repository ISTITUZIONALE

Amyloid β-peptide insertion in liposomes containing GM1-cholesterol domains

note finali coverpage

(Article begins on next page)

05 May 2024

Amyloid β-peptide insertion in liposomes containing GM1-cholesterol domains

Maria Carmela Nicastro[2], Dario Spigolon[1,5], Fabio Librizzi[1], Oscar Moran[3],
Maria Grazia Ortore[4], Donatella Bulone[1], Pier Luigi San Biagio[1], Rita Carrotta[1]

[1]*Italian National Research Council, Institute of Biophysics - Via Ugo La Malfa 153 - 90146 Palermo*

[2]*Italian National Research Council, Institute of Biostructure and Bioimaging - Via Gaifami 18 - Catania*

[3]*Italian National Research Council, Institute of Biophysics - Via De Marini, 6 - 16149 Genova*

[4]*Department of Life and Environmental Sciences, Università Politecnica delle Marche, Ancona, Italy*

[5]*Department of Physics and Chemistry, Università di Palermo, Italy*

ABSTRACT

Neuronal membrane damage is related to the early impairments appearing in Alzheimer's disease due to the interaction of the amyloid β-peptide (Aβ) with the phospholipid bilayer. In particular, the ganglioside GM1, present with cholesterol in lipid rafts, seems to be able to initiate Aβ aggregation on membrane. We studied the thermodynamic and structural effects of the presence of GM1 on the interaction between Aβ and liposomes, a good membrane model system. Isothermal Titration Calorimetry highlighted the importance of the presence of GM1 in recruiting monomeric Aβ toward the lipid bilayer. Light and Small Angle X-ray Scattering revealed a different pattern for GM1 containing liposomes, both before and after interaction with Aβ. The results suggest that the interaction with GM1 brings to insertion of Aβ in the bilayer, producing a structural perturbation down to the internal layers of the liposome, as demonstrated by the obtained electron density profiles.

INTRODUCTION

The accumulation and deposition of the amyloid β-peptide (Aβ) in the neuronal extracellular space and its interaction with neuron membranes (pre- and post-synaptic) are considered crucial steps in the complex neurodegenerative process of brains affected with Alzheimer's disease (AD). In fact, neuronal membrane damage seems to be related to the early impairments appearing in the disease. In neuron plasma membranes are abundant distinct microdomains, rich of cholesterol and gangliosides, so called lipid rafts, considered essential for the membrane fluidity and the electrical and chemical signaling [1]. It has been reported that Aβ is able to bind the ganglioside GM1, that is expressed on the extracellular surface, particularly on synaptic membranes [2]. The complex GM1-Aβ *in vivo* has been identified in cerebral cortices from AD and Down's syndrome subjects, while it was not detected in controls [3]. Lipid rafts and in particular cholesterol associated GM1 clusters can modulate the conversion from unordered to more ordered (α or β) Aβ conformations, by creating a potential endogenous seeds able to onset self assembly on the membrane surface [4-6]. The interaction and the effect on Aβ□□□□□□□□□□□□□□□□□has been widely studied through different techniques in vitro and in silico, trying to understand the mechanism and also highlight the important role of the lipid environment [7-12]. Literature data indicate that the composition of the membrane system, the Aβ form, the physico-chemical conditions during the experiments are all extremely important parameters in determining the behavior of the system, and this explains the quite broad spectrum of reported results. In few studies, the interaction of GM1 with Aβ has been investigated by isothermal titration calorimetry [13-14] and small angle X-ray scattering [15], by using suitable membrane model systems.

In this work we report a study on the interaction of Aβ with liposomes, made of a binary mono-unsatured POPC:POPS lipid combination and 10% w/w of cholesterol, with and without GM1 (5% w/w). This kind of liposomes constitutes a good example of membrane model system, mimicking some properties (dynamics, lipid phase, membrane charge) of the natural membranes under physiological conditions. The interaction was studied by isothermal titration calorimetry (ITC) and small angle X-ray scattering (SAXS), in order to extract both thermodynamic and structural information. Results clearly show that the presence of GM1 is crucial in determining the interaction between Aβ and membranes at a quite low concentration of Aβ (50μM), with a lipid/peptide molar ratio of 300:1. It is noteworthy that in previous literature lower lipid/peptide and lower lipid/GM1 molar ratios were investigated (≈120:1 and 10:1, respectively [15]), hence

the results we obtained are notable. Also, the low Aβ concentration we used allows to prevent aggregation and to single out the interactions between GM1 and freshly dissolved Aβ molecules. The electron density profile obtained from SAXS data analysis indicates that, in the presence of GM1, Aβ is able to produce a perturbation in the lipid bilayer structure, which propagates down to the inner polar region.

MATERIAL & METHODS

Sample Preparation

Synthetic Aβ40 (Polypeptide Group. Product SC869) was pretreated according to the procedure of Fezoui et al. (2000) for improving the reliability of experiments at neutral pH [16].

Aβ40 samples were prepared by dissolving the lyophilized peptide in 50 mM phosphate buffer at pH 7.4 and 20mM NaCl. The initial concentration was about 20% higher than the one chosen for the experiment. Solutions were filtered sequentially through 0.22 μm (Millex-LG syringe filters) and 20 nm filters (Anaspec) and the concentration was measured by tyrosine absorption at 276 nm, using an extinction coefficient of 1390 cm^{-1} M^{-1} [17]. The sample was then diluted to the suited concentration for the experiments.

Phospholipids, POPC (P3017) and POPS (51581), ganglioside GM1 (G7641) and cholesterol (C8667) were purchased from Sigma-Aldrich and used without any further purification. Different liposome compositions were obtained by weighing and mixing in the chosen proportion the different components and then by dissolving the obtained mixture in chloroform. We studied three lipid combination, designed from now on as A (PC:PS=9:1), B (PC:PS:Chol=8.1:0.9:1) and C (PC:PS:Chol:GM1=7.65:0.85:1:0.5). The composition is expressed in mass ratio. Lipid films were obtained by evaporation of the solvent under a very gentle nitrogen flux and in order to remove all chloroform, films were further dried overnight in vacuum in order to remove residual chloroform. A Multi Lamellar Vesicle solution was obtained by hydration of the lipid film with 50mM phosphate buffer with 20mM NaCl at pH7.4. Liposomes were then obtained through extrusion with a mini-Extruder Avestin after 21 passes, by using a couple of 100nm polycarbonate filters. Mass concentration of lipids was known from the lipid film. The recovery of the whole lipid mass from the apparatus was achieved by adding buffer to perform a second extrusion after the one to produce the liposomes used for the experiments, in order to obtain a better estimate of the lipid concentration (see below).

Evaluation of lipid mass loss during extrusion

In order to appreciate if there was a loss of mass during the extrusion step, we extimated the final

concentration of the extruded solution by assuming the starting film mass and using static light scattering. We measured the Rayleigh ratio, I_1 and I_2, relative to the two extruded solutions, step 1 and 2 respectively (see above), after appropriate dilution (d_1 and d_2 respectively, on the order of 100 - 1000). Known the total mass M into the hydrated film, the extruded volumes V_1 and V_2 and the unrecovered volume ΔV, we thus calculated $c_1 = M/V_1 [(1+ ((I_2 d_2)/(I_1 d_1))(V_2+\Delta V)/V_1]$- 1. c_1 is the experimental estimated mass concentration of the solution used in the experiments. In all cases, the reduction of c_1 due to the extrusion procedure was not higher than 10%, compared to the theoretical one $c_0 = M/V_1$.

For both extrusion steps, the particles obtained after the extrusion were found to have, by dynamic light scattering measurements, a comparable and quite narrow size distribution range, characterized by an average hydrodynamic radius of about 75 nm, as obtained making the harmonic average on the distribution.

With the aim to have an idea of the conversion factor between lipid and liposome molar concentrations in our systems we made a rough estimate. We calculated in fact the external surface $S_{Lipo} = 4\pi R_h^2$ and by using the single lipid occupied area for POPC A=0.63 nm^2 [18, 19], we found an average lipid number per liposome $<N_{lip}> = 2 * S_{Lipo}/A$ of about 2.2 10^5.

Static and Dynamic Light Scattering

Liposomes were characterized by Static and Dynamic Light Scattering techniques (SLS and DLS). The extruded sample, after suitable dilution, was placed into a dust-free quartz cell without further filtering and kept at 20^{0}C in the thermostated cell compartment of a Brookhaven Instruments BI200-SM goniometer. The temperature was controlled within 0.1^{0}C using a thermostated recirculating bath. The scattered light intensity and the time autocorrelation function were measured by using a Brookhaven BI-9000 correlator and a 100 mW solid-state laser at λ = 532 nm. Multi-angle Static Light Scattering was performed on the liposome samples in order to obtain the form factor of the nanoparticles in the q range 5 - 29 μm^{-1}. Data were analyzed in terms of two populations of hollow spheres with a fixed layer, ΔR (3.6 nm for samples A and B, and 3.9 nm for C, as obtained from SAXS results) and external and internal radius R_1 and $R_2 = R_1 + \Delta R$, respectively. DLS measurements were performed at 90°, corresponding to q=23 μm^{-1}. Static light scattering data were corrected for the background scattering of the solvent and normalized by using toluene scattering intensity as reference. Toluene Rayleigh ratio was taken as $R_{tol}=28e^{-6}$ cm^{-1}. In DLS experiments, the field autocorrelation function, $g^{(1)}(t) = [g^{(2)}(t)-1]^{1/2}$ was obtained by measuring the intensity correlation function and analyzed by using a smoothing constrained regularization method [20], in order to

determine the distribution of relaxation times according to:

$$g^{(1)}(t) = \int A(\Gamma) \exp(-\Gamma t) d\Gamma \tag{1}$$

where $A(\Gamma)$ denotes the contribution amplitude of the mode with characteristic time Γ^{-1}. The latter is related to the diffusion coefficient by $\Gamma = D q^2$. $A(\Gamma)$ can be expressed also as $A(R_h)$, where R_h is the hydrodynamic radius, by using the Stokes-Einstein relationship $D=k_BT/6\pi\eta R_h$. The distribution obtained by data analysis is intensity weighted. To obtain a number distribution, we considered liposome mass M proportional to R_h^2, a reasonable assumption, given the geometry of the liposomes that can be modeled as spherical shells. The harmonic intensity average radius was obtained from the weighted intensity distribution.

Differential Scanning Calorimetry

Calorimetric experiments were conducted on a DSC (Hart Scientific-Model 707) to characterize the liposomes produced for the experiments of interaction. Measurements were carried out in the temperature range from -12 to 30 °C, with heating rates of 15°C/hour, and different protein concentration (2÷15 mg/ml) in 50 mM phosphate buffer, 20 mM NaCl.

For the measurements 200 µL of sample solution was loaded into the sample cell of the instrument while a matching buffer solution was loaded into the reference cell. Samples and buffers were filtered and degassed in vacuum before loading into the DSC sample cell and reference cell.

The calorimetric enthalpy changes of the transitions (ΔH^{Cal}) were calculated by integrating the area under the peak of the heat capacity (Cp^{trs}) of the transition using the following equation:

$$\Delta H^{Cal} = \int_{T_1}^{T_2} Cp^{trs} dT \tag{2}$$

Where T is the absolute temperature. Tm was estimated as the midpoint of transition.

Isothermal Titration Calorimetry

The heat flow resulting from the binding of the peptide to lipid vesicles was measured using a NANO ITC Low Volume (TA Instruments, USA), with a reaction cell volume of 170 µL. Prior to use, all solutions were degassed under vacuum to eliminate air bubbles. The data were acquired by computer software developed by TA Instruments. All the titration experiments were performed by successive 2µL injections of freshly prepared 73µM Aβ40 into 4mM LUVs solutions (POPC:POPS 9:1; 10%wt Cholesterol and 5%wt GM1 when present), and the interval between injections was 300 sec. All experiments were conducted at 25 °C. Stirring at 280 rpm ensured a good mixing. Each injection produced a heat of reaction, which was determined by

integration of the heat flow tracings. Binding isotherms were corrected by subtracting the corresponding LUV and ligand dilution isotherms.

ITC data were analyzed using the Nano Analyze Data Analysis TA® software. Data fits were obtained using an independent binding model (one-site Independent), for which the analytical solution for the total heat measured (Q) is determined by the formula:

$$Q = \frac{V\,\Delta H}{2K}\left((1 + [Lip]nK + k[L] - \sqrt{(1 + [Lip]nK + [L]K)^2 - 4[Lip]nK^2[L]}\,\right) \qquad (3)$$

where V is the reaction volume, ΔH is enthalpy of binding, [L] is ligand concentration, [Lip] is the total concentration of lipids available for binding ligand, n is the molar ratio of interacting species, and K is the equilibrium binding constant [21]. Gibbs free energy, ΔG, was determined from the binding constant ($\Delta G = -RT\ln K$, where R is the gas constant and T is the absolute temperature in Kelvin) and entropy, ΔS, from $\Delta G = \Delta H - T\Delta S$.

Small angle X-ray Scattering (SAXS)

Liposomes, without and with Aβ were prepared in a phosphate buffer (20mM NaCl, 50 mM phosphate buffer at pH 7.4). Total lipid concentration of liposomes was 15 mM, and Aβ final concentration was 50 μM. (lipid:Aβ ratio 300:1). Small-angle X-ray scattering (SAXS) spectra of membranes were collected at the SAXS beamline of the Elettra Synchrotron (Trieste, Italy). Scattered radiation was recorded in a Pilatus3 hybrid photon counting detector. The sample-detector distance of 1 m covered the range of momentum transfer $0.1 < q < 5.0$ nm^{-1} ($q = 4\pi \sin(\theta)/\lambda$, where 2θ is the scattering angle and $\lambda = 0.154$ nm is the X-ray wavelength; the optical path of the X-ray through the sample is about 1 mm). Data were collected from samples quartz capillaries kept at 25 °C. For each sample, we recorded 30 spectra of 10 s each, with a dead time of 15 s between an acquisition and the next, corresponding to a total of 5 min of data acquisition, and 5.6 min of radiation exposure. Given the random orientation of the vesicles, the detector images were integrated radially with the program Fit2D [22], resulting in the so-called '*I–q* plot', a one-dimensional profile of X-ray intensity *I(q)* versus scattering vector *q*. The comparison of ten successive exposures of an acquisition experiment indicated no changes in the scattering patterns, i.e., no measurable radiation damage to the samples. The scattering data of the buffer, tested before and after each corresponding measured sample, were averaged and used to subtract the background.

SAXS Data Analysis

The structure of the membranes was inferred from their electronic density profiles calculated from the SAXS spectra. In these experiments, the measured X-ray intensity is an average over a polydisperse vesicle population according to Debye scattering theory [23] such that

$$\langle I(q) \rangle = N \langle F(q)^2 \rangle + \langle F(q)^2 \rangle \sum^N \langle cos(q \cdot r_{nn'}) \rangle \tag{4}$$

where $F(q)$ is the bilayer form factor, N is the number of particles (vesicles) and $\boldsymbol{r_{nn'}}$ is the inter-vesicle vector. The first term of equation (4) represents the average scattering of N individual vesicles, while the second term comes from the interference between vesicles and depends on the distance between them, $\boldsymbol{r_{nn'}}$. Because of the low vesicle concentration used in this study, no interference between vesicles is expected [24]. In fact, scattering coming up from the second term becomes significant at $q \ll 0.1$ nm^{-1} [24] that is beyond of the q range utilized here. Thus, the second term of equation (4) could be neglected, and we can use the simple relation:

$$\langle I(q) \rangle \propto \langle F(q)^2 \rangle \tag{5}$$

where N is included in the arbitrary instrumental scaling. The form factor, $F(q)$, is the Fourier transform of the electronic density $\rho(r)$ of the bilayer. To calculate the electronic density we constructed a model of the membrane, and adjusted the parameters of the model to fit its Fourier transform to the experimental SAXS spectra. The electronic density of the vesicle wall can be described by five concentric Gaussian shells [24-28], that include an asymmetric bilayer profile with added decorations on the inner and outer sides of the vesicle wall. The bilayer electronic density profile is modelled by two positive Gaussians, representing the headgroups of the two lipid leaflets (*in* and *out*, respectively) and a negative Gaussian representing the hydrophobic core (*tail*). The asymmetric distributed material extending beyond the bilayer towards the internal or external sides of the vesicle (*inner* and *outer*) are modelled by concentric Gaussians attached to the inner and outer sides of the bilayer, respectively. The electronic density of the bilayer profile as a function of the distance r is given by:

$$\rho(r) = \sum_{k=1,5} \rho_k \, exp \left[\frac{-(r-\delta_k)^2}{2\sigma_k^2} \right] \tag{6}$$

7

with the peak position δ_k, amplitude ρ_k, and width σ_k with *k* indicating *in, out, tail, inner, outer*, for each of the three Gaussians representing the headgroups of the two leaflets and the phospholipid tail region, and the inner and outer membrane decorations, respectively. The radius *R* is the distance defined from the center of the vesicle to δ_{tail}. Thus, we define $\varepsilon_k = \delta_k - R$, and therefore we fixed $\varepsilon_{tail} = 0$. The membrane thickness is characterised by the total thickness *d* of the bilayer structure:

$$d = \left[\epsilon_{\mathrm{in}} - \sigma_{\mathrm{in}}\sqrt{2\pi}\right] - \left[\epsilon_{out} + \sigma_{out}\sqrt{2\pi}\right] \tag{7}$$

In other SAXS data analysis methods, where the electronic density is based on the chemical composition of the bilayer, the membrane thickness is calculated as the distance between the water-lipid interphase, explicitly defined on the membrane models [19].

SAXS data allow to measure the scattering contrast $\Delta\rho = \rho(r) - \rho_{solvent}$. This analysis provides the relative amplitudes of each bilayer feature, not the absolute amplitudes, and the magnitude of $\rho_{solvent}$ is arbitrary and set equal to zero. The electronic density of the two peaks representing the headgroups were defined to be $\rho_{in,out} > 0$, and the peak that represents the lower electronic density of the bilayer, plausibly corresponding to the methyl groups of the phospholipids was fixed to $\rho_{tail} = -1$ [29]. These two assumptions reduced the parameter dependency of the fitting procedure and also provided a means of comparing the models since all results were normalized to the central region of the bilayer. Notice that the Gaussians representing the bilayer profile and the protein shells inter-penetrate to some extent. For a perfectly spherical, radially symmetric vesicle composed of *n* Gaussian shells, the form factor $\langle F(q)^2\rangle = F(q)F(q)^*$ is obtained from the radially symmetric Fourier transform of equation 5. We used a normalized ensemble average over $F(q)^2$ [24, 27-28], resulting in

$$\langle F(q)^2\rangle = \zeta\left\{\frac{1}{q^2}\sum_{k,k'}(R+\epsilon_k)(R+\epsilon'_k)\rho_k\rho'_k\sigma_k\sigma'_k \times exp\left[-q^2\left(\frac{\sigma_k^2+\sigma_{k'}^2}{2}\right)\right]cos[q(\epsilon_k-\epsilon'_k)]\right\} \tag{8}$$

where $F(q)^2$ is the form factor and ζ is a proportionality factor. Note that equation 8 is an approximation valid only in the region 0.1 nm^{-1} > q > 10 nm^{-1}, where intensity, arising from intra-bilayer features, dominates the scattering curve. The derivation of the expression in equation 8, obtained from a normalized ensemble average over $F(q)^2$ utilizing a Gaussian weight to describe the distribution of vesicles with radii *R'*, average radius *R* and standard deviation σ_R, is described in the Appendix A of the article of Brzustowicz and Brunger (2005) [25]. The data

fitting procedure utilized the non-linear, least-squares Levenberg-Marquardt fitting (NLSF) algorithm to minimize χ^2 (IgorPro, Wavemetrics, Lake Oswego, OR, USA):

$$\chi^2 = \sum_j \frac{I(q_j) - \hat{I}(q_j)^2}{\sigma(q_j)} \tag{9}$$

where $\hat{I}(q_j)$ is a fitted value (model value) for q_j, $I(q_j)$ is the measured data value for the jth point and $\sigma(q_j)$ is an estimate of the standard deviation for $I(q_j)$. The goodness of the fit was characterized by the correlation coefficient r^2. The electronic density profile of the lipid vesicle wall was obtained with high accuracy fitting the model over the experimental data. This method allows also to having a good estimate of the average vesicle radius.
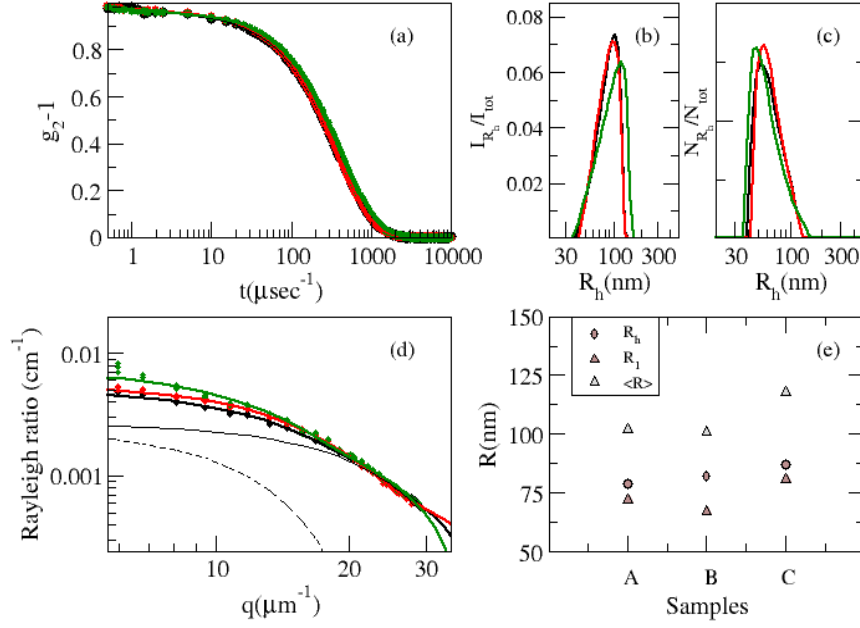
RESULTS

The interaction of Aβ with liposomes, made of monounsaturated lipids, with a composition that can mimic the surface charge of plasma membrane, in the presence of 10% cholesterol and 5% ganglioside GM1 was studied by ITC and SAXS. A preliminary characterization of the liposome systems studied was performed by Light Scattering and DSC. We remind here the composition as mass ratio of the three investigated liposome samples: A (PC:PS=9:1), B (PC:PS:Chol=8.1:0.9:1) and C (PC:PS:Chol:GM1=7.65:0.85:1:0.5).

Liposome characterization

Static and Dynamic Light Scattering

All samples were firstly characterized by light scattering. In fig.1, the upper panels report the Dynamic Light Scattering results. The intensity autocorrelation functions (fig.1a) were analyzed according to the expression (1), and the resulting distributions of the hydrodynamic radii are reported in panel (b) (intensity weighted) and in panel (c) (number weighted). In the lower panels the multi-angles Rayleigh ratio, together with the analysis, performed according to the presence of two populations of spherical shells with thickness ΔR (set 3.6nm for A and B and 3.9nm for C liposomes) and external and internal radius R_1 and $R_2 = R_1 - \Delta R$ respectively, are reported (d); The single contributions coming from the two shells are also reported, as an example for the sample A. It is worth to note that at i.e. the q value corresponding to our DLS measurements for the determination of the hydrodynamic radius, the scattering arising from the larger species is almost negligible with respect to the scattering contribution coming from the small ones. As a consequence, the hydrodynamic radius obtained by DLS at $q=23\mu m^{-1}$, is comparable to the radius of the smaller species observed by multi-angle SLS (see fig. 1e).

Figure 1: Dynamic (a, b, c) and Static (d, e) Light scattering characterization: $[g_1(t)]^2$ for A (black), B (red) and C (green) in panel (a); Continuous lines are the data fits according to eq.(1). Size distributions resulting from the analysis of $g_1(t)$, as it comes from the analysis, i.e. intensity weighed (b) and corrected to obtain a number distribution (c). Multi-angle scattering (d). Thick continuous lines show the fit functions according to the two shells model for A, B and C. The light and hatched black lines represents the two components in the A analysis. Radii obtained from the analysis of DLS and SLS results.

Differential Scanning Calorimetry

The interaction between cholesterol and phospholipids has been widely studied by DSC technique [30, 31]. First, we characterized LUV made of only POPC and POPC:POPS (9:1), without and with cholesterol. The resulting molar heat capacity is reported in Fig.2a. (black and blue line, respectively). As evident in the figure, in these first two cases, we observe a phase transition, for which the integral and temperature corresponding to the maximum of the thermograph were estimated giving a ΔH^{Cal} of 10.5 kJ/mole and 20 kJ/mol, and a Tm of -1.4°C and 0.55°C respectively. These parameters corresponding to the main transition, from gel to crystal liquid. When cholesterol is added (15%w/w) to the phospholipid components, the main endothermic transition of the phospholipids disappears (Fig. 2a, red line). Cholesterol exerts a strong perturbing effect on phospholipid bilayers, indicating a marked growth in the orientational disorder of the phospholipid chains, as reported in literature [32].

Fig.2b reports the heat capacity for liposomes A, at two different concentrations, for liposomes A with 15% of cholesterol, and liposomes C, containing also GM1. A transition is observed only in

liposomes A, indicating again a high disorder of the phospholipid chains in the bilayer in the presence of cholesterol and both cholesterol and GM1 (red and green line respectively).
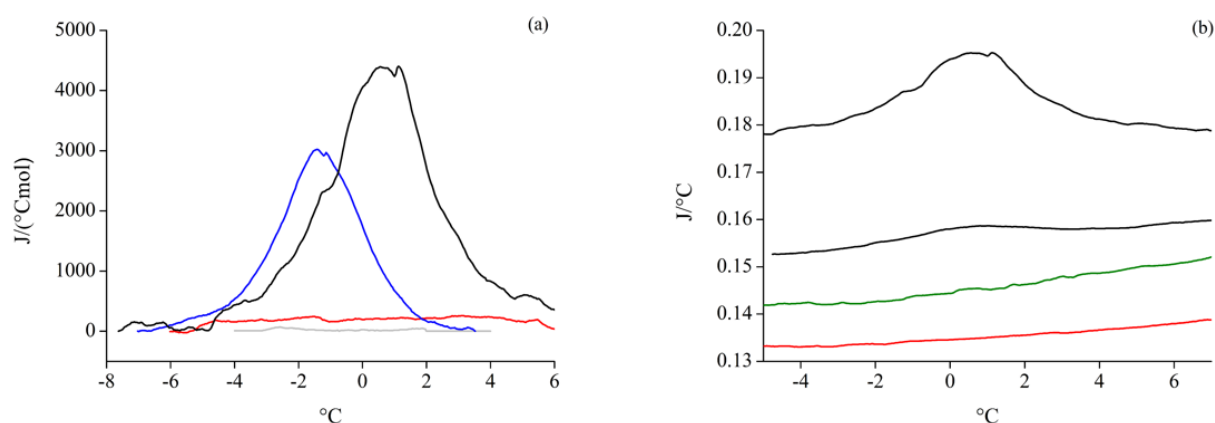

Figure 2: DSC thermographs of phospholipid vesicles: (a) Molar heat capacity, after baseline subtraction, for 15 mg/ml solutions of POPC LUV (blue), POPC:POPS LUV (black), POPC:POPS + 15% Cholesterol (red) and 28% Cholesterol (grey); (b) Raw heat capacity of POPC:POPS LUV (black) at 15mg/ml (top) and 2.3mg/ml (below), 2.3mg/ml POPC:POPS + 15% Cholesterol (red) and 2.3mg/ml POPC:POPS + 10% Cholesterol + 5% GM1 (green).

Interaction Studies

The interaction between Aβ and liposomes of different type, A, B and C has been investigated by Isothermal Titration Calorimetry and Small Angle X-ray Scattering, in order to study both the thermodynamics of the interaction and changes in the structure of the liposome double layer due to Aβ peptide presence.

ITC

Fig. 3a reports the rate of heat flow measured under titration of liposomes B and C. Results show that the addition of Aβ to solution of liposomes, containing GM1 ganglioside and cholesterol, leads to a heat exchange, inferring an interaction between the two systems (green line). In contrast, no heat exchange occurs in the absence of GM1. The binding isotherms corresponding to ITC experiments for the three samples A, B and C are reported in fig. 3b. The simultaneous presence of cholesterol and GM1 promotes the interaction with the Aβ peptide, with a strong exothermic binding enthalpy, thus indicating the recruitment of Aβ toward the membrane.
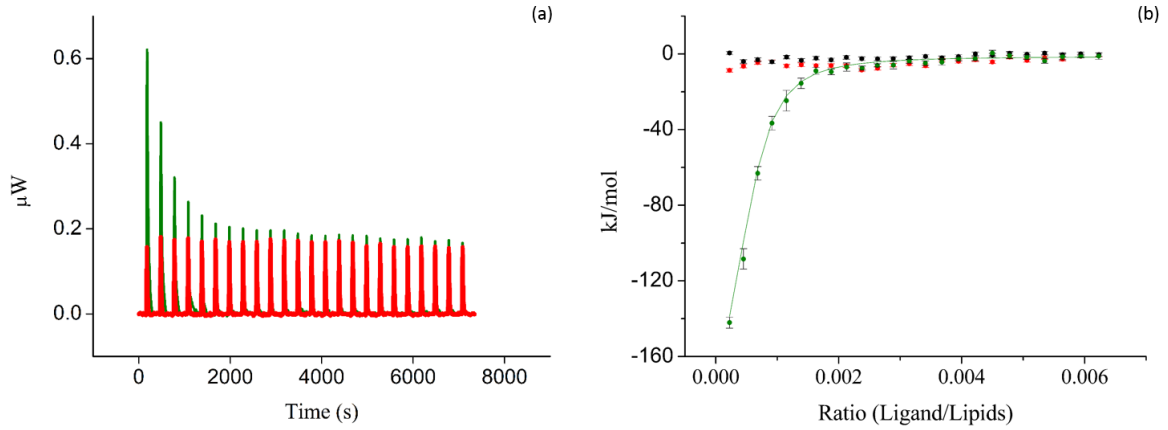
Figure 3: (a) Heat rate flow in the titration of 73μM Aβ40 in B LUVs containing (red) and C LUVs (green). (b) Binding isotherms obtained using Incremental Injection ITC, titrating (2μL) 73μM of Aβ40 into the three different liposome solutions (4mM): A LUV (black); B LUV (red); C LUV (green). Where not visible, error bars are inside the experimental points dimension. The line represents the binding curve obtained by the analysis according to one-site Independent binding model reported in eq. (2).

The binding isotherm can be described by using a one-site independent binding model, according to the equation (2). Fit to data is reported in Fig. 3b (green line). The fit to the one-site binding model yields an association constant $K_a = (1.64 \pm 0.37)\ 10^6\ M^{-1}$, an exothermic binding enthalpy $\Delta H = (-202.5 \pm 19.7)$ kJ/mol, and a binding entropy $\Delta S = (-0.56 \pm 0.07)$ kJ/mol·K. The change of the free energy due to peptide binding is $\Delta G = (-35.5 \pm 0.6)$ kJ/mol. The binding stoichiometry was $n = (5.0 \pm 0.3) \times 10^{-4}$ (Aβ/lipid ratio, corresponding to ~0.02 Aβ/GM1 ratio and approximately to 100 Aβ/liposome ratio). Results clearly indicate that fresh Aβ has a high affinity only for GM1-cholesterol liposomes, but not for liposomes with cholesterol alone. Furthermore, the interaction results to be enthalpy driven, and in higher ionic strength environments it is vanishing (data not shown), thus suggesting an essential role for electrostatic interactions in the binding. Previous studies on charged liposomes are consistent with these findings [14].

SAXS

In SAXS measurements, Aβ peptide concentration was chosen in order to have an Aβ/lipid ratio of 0.0033. According to ITC results (see Fig. 3b), this value is high enough to observe a good interaction, still being sufficiently low to prevent unwanted peptide aggregation and/or oligomerization. Fig. 4a shows the SAXS spectra obtained from samples B and C, before and

after mixing with Aβ. Spectra are reported in an arbitrary intensity scale and translated in order to better visualize the different profiles. The addition of GM1 to the LUV introduces a modification on the structure of the liposomes, as results from substantial differences which can be observed in the range 1.5-3.5 nm^{-1} when comparing the bilayers B and C (Fig. 4a, red and green lines, respectively). The SAXS spectra recorded from B liposomes in the presence or in the absence of the Aβ peptide are quite undistinguishable (Fig. 4a, red and magenta lines, respectively), suggesting that B liposomes do not interact with the peptide at least in our experimental conditions. Conversely, the comparison of SAXS spectra of C liposomes with or without Aβ shows striking differences, especially in the spectra minimum around 2.5 nm^{-1} (Fig. 4a, green and cyan lines, respectively). The analysis of the data according to the multi-Gaussian model described in the methods section, allows the construction of the electron density profiles of the bilayer of vesicle walls (Fig. 4b). A distinctive asymmetry in the bilayer comes out, for all the samples, most probably due to the membrane curvature [24, 28]. In the presence of GM1 the electron density shows up an inversion of sign close to the vesicle surface, which is modeled by a low intensity negative Gaussian, consistent with a protrusion from the shell, with hydrophobic tendency. This affects the external radius of the C liposomes, in agreement with DLS results. Interestingly, the presence of Aβ brings about a lowering of the electron density, probably coming from neutralization of charges, due to the interaction and the disappearance of the negative Gaussian once the peptide is inserted. The peptide is eventually perturbing the double layer down to the inner polar layer.
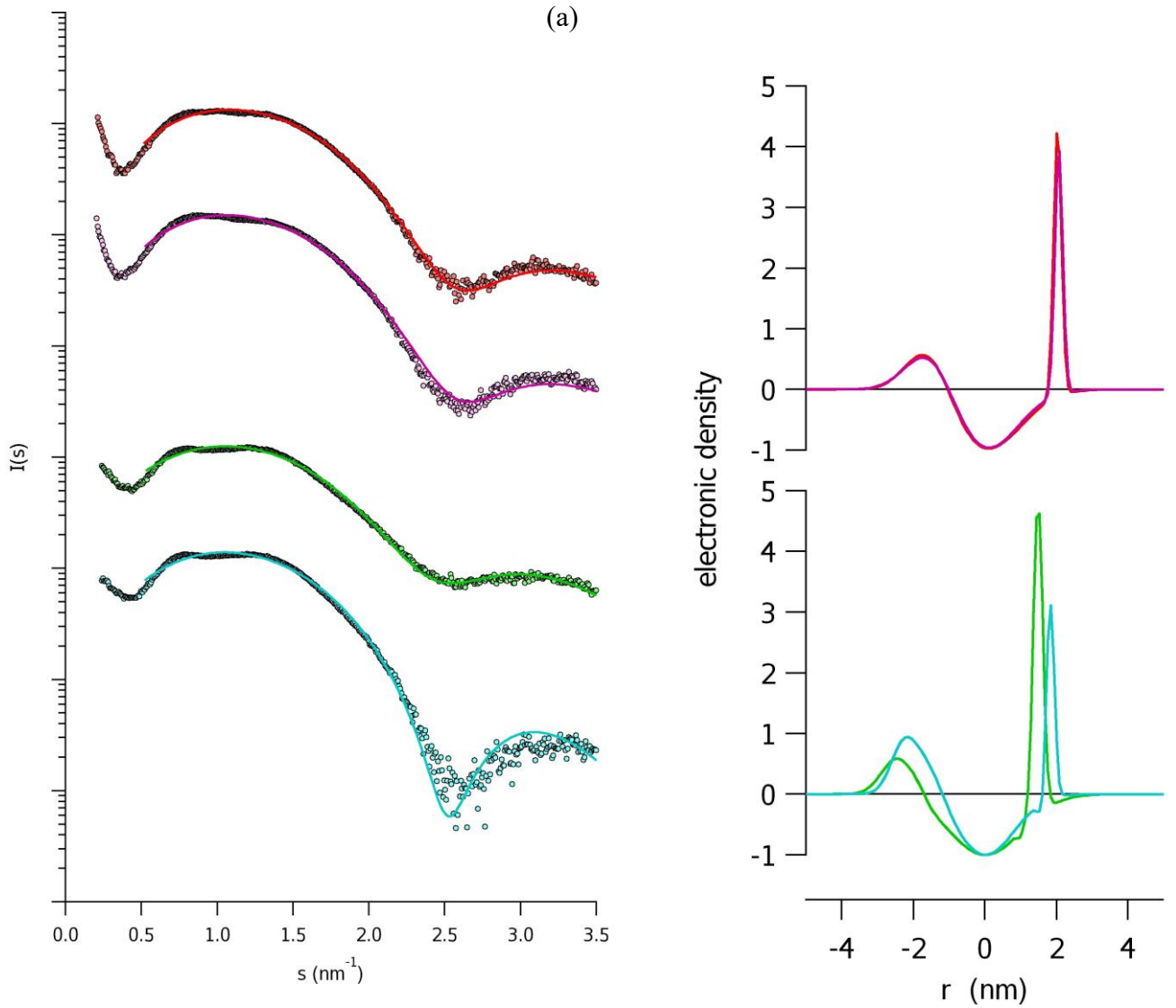
Figure 4: (a) SAXS spectra of the LUVs B and C before (red and green, respectively) and after mixing with Aβ☐☐☐☐☐☐☐☐a☐☐☐☐☐☐☐☐☐☐☐☐☐☐☐☐☐☐☐☐☐☐☐☐. Lipid concentration was 15mM and, when present, Aβ☐concentration was 50mM. Continuous lines represent the best fitting of data, according to the multi-Gaussians model. (b) Electronic density profiles for sample B and C before (red and green, respectively) and after mixing with Aβ (β☐☐☐☐☐☐☐☐a☐☐☐☐☐☐☐☐☐☐☐☐☐☐☐☐☐☐☐☐☐☐☐☐), calculated from the experimental SAXS data according to the multi-Gaussians model.

The structural parameters, calculated from the calculated electronic density distribution are reported in Table I. It is important to note that the analysis has been performed in a recursive way in order to use all accessible experimental information. In fact, SAXS modeling analysis

was started by using the LUV dimensions, as obtained by DLS measurements (they were let free to change in the last runs), and in multi-angle light scattering analysis we used the layer thickness obtained by the gaussians model SAXS analysis.

Table I: Structural parameters resulted from the calculation of the electronic density of the vesicle lipid bilayers by multi-Gaussian model. Data represents the values ± standard deviation. The correlation coefficient represents the goodness of the fitting of the original SAXS data with the model.

	B	**B+Aβ**	**C**	**C+Aβ**
correlation coefficient	0.9951	0.9928	0.9933	0.9935
bilayer thickness (nm)	3.59 ± 0.11	3.59 ± 0.06	3.91 ± 0.08	4.10 ± 0.11
vesicle radius (nm)	76.8 ± 1.7	80.2 ± 1.7	81.9 ± 1.8	86.3 ± 1.7

DISCUSSION

We reported here a characterization and an interaction study on membrane model systems with the freshly dissolved Aβ-peptide. The LUV composition has been chosen by perturbing a model liposome made of POPC, which is the most abundant component of natural membranes. POPS has been added to take into account the membrane charge, cholesterol as a main realistic membrane component and GM1 in vivo it is found to play a fundamental role in the interaction Aβ peptide/membrane and further aggregation seeding, together with cholesterol.

Our results show a structural asymmetry between the outer and inner leaflet, that is a naturally occurring property of the cellular membranes [33]. The X-ray scattering profile reflects the asymmetry in the characteristic nonzero minima pattern [34]. In the system we chose, that well simulate some peculiar properties of a natural membrane, we found a cholesterol dependent interaction involving GM1 and Aβ□□□□□□□a $K_A = (1.64 \pm 0.37)$ 10^6 M^{-1}. Studies by Surface Plasmon Resonance, reporting a value of 0.8 10^6 M^{-1}, with 20% GM1 in liposomes made of DMPC [13] and 1.2 10^6 M^{-1}, with a relative composition DPPC:GM1:Chol of 5:4:1 in mass [14] agree with our value, considering the different lipid composition, and in particular the absence of cholesterol in liposomes studied in Valdes-Gonzalez et al. (2003).

In our SAXS study we used a quite low ratio Aβ/Lip=0.0033, as suggested by ITC titration results. Under such conditions we are sure to avoid aggregation and to focalize only onto the interaction between the membrane and the Aβ molecules. Indeed, studies on Aβ40 fibrillogenesis show that in these conditions stirring is needed for the onset of the aggregation process [35, 36], at least in the time course of our interaction experiments. In a previous study some of us studied by AFM spectroscopy the interaction between different aggregation states of Aβ and a supported planar bilayer (PC:PS=9:1). A major topological effect, appearing like a lipid depletion, was observed under interaction with oligomers/protofibrils, while no effects at all were detected for mature fibrils and only minor changes for fresh Aβ. In this work we do not observe any interaction for freshly dissolved Aβ with analogous lipid composition liposomes (sample A). However, we have to consider that the number of peptide molecules per surface unit in the two studies was considerably different, being much higher (about 500 fold) for the planar bilayer study reported in ref [37].

In our study, the detected structural change in sample C consist in an average increase of the layer thickness, suggesting that the molecular interactions prompt the recruitment of the peptide to the raft lipid domains, which are rich in GM1 and cholesterol. Interestingly, the whole bilayer is perturbed by the interaction. According to a recent study reporting SAXS and neutron spin-echo measurements, the phase state of the lipid system used for the interaction is a crucial point in order to appreciate bilayer changes. The interaction of fresh Aβ with ternary LUV (PC:Chol:GM1) was investigated by detecting both the structure and dynamics of the bilayer: bending-diffusion motions were suppressed but only for the system in L_α (disordered) phase, while the structure was not altered [15]. This difference in the results could be caused by the formation of Aβaggregates, that are not able in this case to penetrate the lipid bilayer, being in fact the Aβ concentration used by Hirai and collaborators, as well as the peptide/lipid ratio, significantly higher (~200 µM) in respect to our study [15].

In a series of calcein release experiments, we did not observe any membrane permeability when adding Aβ peptide, even for GM1 containing liposomes (data not shown). Nevertheless, the calorimetric and SAXS data here reported clearly indicate an interaction between the membrane and the peptide. Put together these results indicate that the interaction does not lead to a membrane destabilization or loosening or to even a detergent effect of the peptide.

Molecular simulation studies coupled also to physico-chemical interaction characterization have given a possible interpretation of the interaction molecular mechanism involving Aβ, GM1 and cholesterol [7]. According to this study the domain Aβ5-16 is interested in the binding to the ganglioside, while the domain Aβ22-35 is linked to cholesterol into the bilayer, determining a

partial insertion of the peptide in the lipid raft. Cholesterol is crucial in this model, being responsible of a ganglioside conformational change, which enhances its affinity to the Aβ peptide [5].

CONCLUSION

We studied the interaction of fresh Aβ with LUV systems, whose composition well mimics a membrane asymmetric system. An interaction between Aβ and GM1 containing liposomes has been measured, in the presence of 10% (w/w) cholesterol. Results suggest that the peptide is recruited in the membrane. The peptide-GM1 interaction, crucially regulated by cholesterol, leads to structural changes in the bilayer down to the inner leaflet. These results confirm the important role that such a binding can play in tuning the structural and dynamic properties of the membrane.

ACKNOWLEDGEMENTS

REFERENCES

[1] H. Hering, C.C. Lin, M. Sheng, Lipid rafts in the maintenance of synapses, dendritic spines, and surface AMPA receptor stability, J. Neurosci. 23(8) (2003), 3262-3271, doi: 10.3389/fnbeh.2014.00104.

[2] K. Yanagisawa and Y. Ihara, K., Ganglioside-bound amyloid β-Protein in Alzheimer's Disease brain, NeuroBiol Aging 19 (1S) (1998), S65-S67.

[3] K. Yanagisawa, A. Odaka, N. Suzuki, Y. Ihara, GM1 ganglioside–bound amyloid β–protein (Aβ): A possible form of preamyloid in Alzheimer's disease, Nature Med. 1 (1995), 1062-1066, http://dx.doi.org/10.1038/nm1095-1062

[4] K. Matsuzaki, How do membranes initiate Alzheimer's Disease? Formation of toxic amyloid fibrils by the amyloid β-protein on ganglioside clusters, Acc. Chem. Res. 47 (8) (2014) 2397–2404, doi: 10.1021/ar500127z.

[5]   A. Kakio, S.I. Nishimoto, K. Yanagisawa, Y. Kozutsumi, K. Matsuzaki, Cholesterol-dependent formation of GM1 ganglioside-bound amyloid beta-protein, an endogenous seed for Alzheimer amyloid, J. Biol. Chem. 276 (27) (2001), 24985-24990, doi: 10.1074/jbc.M100252200.

[6]   J. McLaurin, T. Franklin, P.E. Fraser, A. Chakrabartty, Structural transitions associated with the interaction of Alzheimer beta-amyloid peptides with gangliosides, J. Biol. Chem. 273(8) (1998), 4506-4515, doi: 10.1074/jbc.273.8.4506.

[7]   J. Fantini, Y. Nouara, N. Garmy, 2013 Cholesterol accelerates the binding of Alzheimer's β-amyloid peptide to ganglioside GM1 through a universal hydrogen-bond-dependent sterol tuning of glycolipid conformation, Front. Physiol. 4 (2013), 120, doi: 10.3389/fphys.2013.00120.

[8]   L.P. Choo-Smith, W.K. Surewicz, FEBS Letters 402 (2-3) (1997), 95-98, doi:10.1016/S0014-5793(96)01504-9.

[9]   B. Kurganov, M. Doh, N. Arispe, N. Aggregation of liposomes induced by the toxic peptides Alzheimer's Abetas, human amylin and prion (106-126): facilitation by membrane-bound GM1 ganglioside, Peptides 25 (2) (2004), 217-232, doi:10.1016/j.peptides.2004.01.001.

[10] P.K. Mandal, J.W. Pettegrew, Alzheimer's disease: NMR studies of asialo (GM1) and trisialo (GT1b) ganglioside interactions with Abeta(1-40) peptide in a membrane mimic environment, Neurochem. Res. 29 (2) (2004), 447–453, DOI: 10.1023/B:NERE.0000013750.80925.25

[11] Y. Tashima, R. Oe, S. Lee, G. Sugihara, E.J. Chambers, M. Takahashi, T. Yamada, The effect of cholesterol and monosialoganglioside (GM1) on the release and aggregation of amyloid beta-peptide from liposomes prepared from brain membrane-like lipids, J. Biol. Chem. 279 (17) (2004), 17587–17595, doi: 10.1074/jbc.M308622200.

[12] T.L. Williams, L.C. Serpell, Membrane and surface interactions of Alzheimer's Aβ peptide -insights into the mechanism of cytotoxicity, FEBS J. 278 (20), 3905-3917, DOI: 10.1111/j.1742-4658.2011.08228.x.

[13] T. Valdes-Gonzalez, J. Inagawa, T. Ido, Characterization of the interactions of ß-amyloid peptides with glycolipid receptors by surface plasmon resonance, Spectroscopy 17 (2-3) (2003), 241-254.

[14] M.S. Lin, H.M. Chiu, F.J. Fan, H.T. Tsai, S.S Wang, Y. Chang, W.Y. Chen, Kinetics and enthalpy measurements of interaction between beta-amyloid and liposomes by surface

plasmon resonance and isothermal titration microcalorimetry, Colloids Surf. B Biointerfaces 58 (2) (2007) 231–236, doi:10.1016/j.colsurfb.2007.03.014.

[15] M. Hirai, R. Kimura, K. Takeuchi, M. Sugiyama, K. Kasahara, N. Ohta, B. Farago, A. Stadler, G. Zaccai, Change of dynamics of raft-model membrane induced by amyloid-β protein binding, Eur. Phys. J. E 36 (7) (2013), 74, doi: 10.1140/epje/i2013-13074-3.

[16] Y. Fezoui, D.M. Hartley, J.D. Harper, R. Khurana, D.M. Walsh, M.M. Condron, D.J. Selkoe, P.T.Jr. Lansbury, A.L. Fink, D.B. Teplow, An improving method of preparing the amyloid beta-protein for fibrillogenesis and neurotoxicity experiments, Amyloid 7 (3) (2000) 166–178, DOI: 10.3109/13506120009146831.

[17] H. Edelhoch, Spectroscopic determination of tryptophan and tyrosine in proteins, Biochemistry 6 (7) (1967) 1948-1954, DOI: 10.1021/bi00859a010.

[18] A. Dickey, R. Faller, Examining the contributions of lipid shape and headgroup charge on bilayer behavior, Biophys. J. 95 (6) (2008), 2636-2646, doi: 10.1529/biophysj.107.128074.

[19] Kucerka, N., Nieh, M.-P., Katsaras, J. Fluid phase lipid areas and bilayer thicknesses of commonly used phosphatidylcholines as a function of temperature, BBA 1808 (11) (2011), 2761-2771. doi: 10.1016/j.bbamem.2011.07.022.

[20] Stepanek, P. In Dynamic Light Scattering: The method and some applications; (Brown, W., Ed.; Clarendon Press: Oxford, UK, 1993), p. 177.

[21] E. Freire, O.L. Mayorga, M. Straume, Anal. Chem. 62 (1990), 950A–958A, DOI: 10.1021/ac00217a715.

[22] A.P. Hammersley, S.O. Svensson, M. Hanfland, A.N. Fitch, D. Häusermann, Two-Dimensional Detector Software: From Real Detector to Idealised Image or Two-Theta Scan, High Pressure Research, 14 (1996), 325-248, DOI: 10.1080/08957959608201408.

[23] A. Guinier, X-ray Diffraction in Crystals, Imperfect Crystals, and Amorphous Bodies, (Courier Dover Publications, San Francisco and London, 1963).

[24] M.R. Brzustowicz, A.T. Brunger, X-ray scattering from unilamellar lipid vesicles, J. Appl. Cryst. 38 (2005), 126-131, doi:10.1107/S0021889804029206.

[25] S. Castorph, L. Arleth, M. Sztucki, U. Vainio, S.K. Ghosh, M. Holt, R. Jahn, T. Salditt, Synaptic Vesicles Studied by SAXS: Derivation and Validation of a Model Form Factor, J. Phys.: Conf. Ser. 247 (1) (2010), 012015, doi:10.1088/1742-6596/247/1/012015.

[26] S. Castorph, D. Riedel, L. Arleth, M. Sztucki, R. Jahn, M. Holt, T. Salditt, Structure parameters of synaptic vesicles quantified by small-angle x-ray scattering, Biophys. J. 98 (7) (2010), 1200-1208, doi: 10.1016/j.bpj.2009.12.4278.

[27] D. Baroni, O. Zegarra-Moran, O. Moran, Functional and pharmacological induced structural changes of the cystic fibrosis transmembrane conductance regulator in the membrane solved using SAXS, Cell. Mol. Life Sci. 72 (7) (2015), 1363-1375, doi: 10.1007/s00018-014-1747-4.

[28] D. Baroni, O. Zegarra-Moran, A. Svensson, O. Moran, Direct interaction of a CFTR potentiator and a CFTR corrector with phospholipid bilayers, Eur. Biophys. J. 43 (6-7), 341-346, doi: 10.1007/s00249-014-0956-y.

[29] G. Pabst, M. Rappolt, H. Amenitsch, P. Laggner, Structural information from multilamellar liposomes at full hydration: full q-range fitting with high-quality X-ray data, Phys. Rev. E 62 (3), 4000-4009, http://dx.doi.org/10.1103/PhysRevE.62.4000.

[30] J.B. Finean, Interaction between cholesterol and phospholipid in hydrated bilayers, Chem. Phys. Lipids 54 (3-4) (1990), 147-156, doi:10.1016/0009-3084(90)90008-F.

[31] S. Bhattacharya, S. Haldar, Interactions between cholesterol and lipids in bilayer membranes. Role of lipid head group and hydrocarbon chain-backbone linkage, Biochim. Biophys. Acta 1467 (1) (2000) 39-53, doi:10.1016/S0005-2736(00)00196-6.

[32] T.P. McMullen, R.N. Lewis, R.N. McElhaney, Comparative Differential Scanning Calorimetric and FTIR and 31PP-NMR Spectroscopic Studies of the Effects of Cholesterol and Androstenol on the Thermotropic phase Behavior and Organization of Phosphatidylcholine Bilayers, Biophys. J. 66 (3) (1994), 741-752.

[33] G. van Meer, D.R. Voelker, G.W. Feigenson, Membrane lipids: where they are and how they behave, Nat. Rev. Mol. Cell Biol. 9 (2008), 112-124, doi:10.1038/nrm2330.

[34] N. kucerka, M.P. Nieh, J. Katsaras (2010), in: Advances in Planar Lipid Bilayers and Liposomes, Vol. 12, (Academic Press, 2010), pp 201-235.

[35] R. Carrotta, C. Canale, A. Diaspro, A. Trapani, P.L. San Biagio, D. Bulone, Inhibiting effect of α_{s1}-casein on Aβ_{1-40} fibrillogenesis, Biochim. Biophys. Acta 1820 (2) (2012), 124-132, doi:10.1016/j.bbagen.2011.11.010.

[36] C. Corsale, R. Carrotta, M.R. Mangione, S. Vilasi, A. Provenzano, G. Cavallaro, D. Bulone, P.L. San Biagio, Entrapment of Aβ(1-40) peptide in unstructured aggregates, J. Phys. Condens. Matter 24 (24) (2012), 244103, doi: 10.1088/0953-8984/24/24/244103.

[37] C. Canale, S. Seghezza, S. Vilasi, R. Carrotta, D. Bulone, A. Diaspro, P. L. San Biagio, S. Dante, Different effects of Alzheimer's peptide Aβ(1–40) oligomers and fibrils on supported lipid membranes, Biophys. Chem. 182 (2013) 23–29, doi:10.1016/j.bpc.2013.07.010.

Graphical Abstract